*Progress In Electromagnetics Research M, Vol. 21, 1–17, 2011*

# A NEW ACCURATE MODEL OF HIGH-IMPEDANCE SURFACES CONSISTING OF CIRCULAR PATCHES

**D. Ramaccia*, A. Toscano, and F. Bilotti**

Department of Applied Electronics, "Roma Tre" University, Via della Vasca Navale, Rome 84-00146, Italy

**Abstract**—In this paper, we consider a dense array of metallic circular patches printed on a electrically thin metal-backed dielectric substrate. Since the sub-wavelength dimensions, the array and the metal-backed substrate can be described in terms of a lumped capacitance and a lumped inductance, respectively. Around the resonant frequency, the structure, known as high-impedance surface, reflects totally an incident electromagnetic wave with zero shift in phase. Due to this property, it is widely employed in antenna systems as compact back reflector with improved performances with respect to typical metal reflector. Starting from the concept of the grid capacitive reactance of a planar array of squared patches and its related formulas, we investigate on the field distribution on the array plane and properly modify the formulas for the case of the circular patches. We present two new analytical formulas which can be effectively used for the fast design of 2D-isotropic circular HISs. In order to validate the models, we compare the resonant frequency of the array obtained through our approaches to the one resulting from full-wave numerical simulations and from other analytical methods available in the open technical literature.

## 1. INTRODUCTION

In the past two decades, the development of wireless communication systems has been possible thanks to significant progress in the fields of electronics and applied electromagnetics. Device miniaturization, superior performances with respect to the state-of-the-art solutions, and low production costs represent the main challenges driving current academic and industry efforts. For what concerns the radiating segment of wireless systems, miniaturization and low-cost solutions are commonly achieved exploiting microstrip printed technology.

*Received 9 May 2011, Accepted 15 August 2011, Scheduled 14 September 2011*

* Corresponding author: Davide Ramaccia (dramaccia@uniroma3.it).

In order to enhance the performances and reduce the size of the radiating systems, antennas can be properly loaded by artificial materials or surfaces [1–5], among which include the so-called metamaterials and metasurfaces, exhibiting functionalizing properties [6–14]. For instance, in order to reduce the thickness of printed antennas and enhance the performances in terms of efficiency and gain, it is possible to use the concept of High-Impedance Surfaces (HISs) [15], capable of highly reduced propagation of surface waves trapped within the substrate. An HIS is a metasurface consisting of a planar array of metallic patches printed on a metal-backed dielectric substrate. Provided that the array periodicity is electrically small, as well as the dimension of the individual particle representing the array unit-cell, an HIS can be represented in terms of its homogenized surface impedance [15]. At and around its resonant frequency, an HIS approximately behaves as a perfect magnetic wall, leading to several interesting applications in the antenna field [15–19]. Shape and dimensions of the individual patch element represent the key parameters for the design of an HIS and the synthesis of its frequency response. Generally, patch elements are arranged in a dense array and exhibit squared [15], hexagonal [16], and rectangular [20] shapes.

In this paper, we refer to an HIS made of a grounded dielectric thin slab with a dense array of circular patches printed on top. Such a configuration is particularly appealing due to its 2D isotropic response on the array plane. The sub-wavelength periodicity of the array and thickness of the substrate, the structure can be studied in the quasi-static regime and consequently in terms of a lumped elements: the metallic patch array can be described as a capacitive reactance, the metal-backed substrate as a inductive one. The shape of the patch element affects the value of the capacitive reactance that need to be properly defined for the geometry under study, i.e., circular in this case. It is possible to find two different approaches in the open technical literature: the first considers the dense array as an frequency selective surfaces (FSSs) in long-wavelength regime [21], and the latter defines the electrically small individual patches in terms of an electric dipoles represented through its electric polarizability [22, 23]. Both define a lumped impedance, that in the case of an array of perfect conducting metallic disks, is capacitive. The sub-wavelength-FSS-based model [21] is derived approximating the Floquet theory under the assumption that the periodicity is few tenths of the operating wavelength. On the contrary the polarizability-based model [23] assumes that the inclusions are so electrically small that they can be described in terms of an electric dipoles, losing the information about the geometry of the inclusion itself.

The aim of this paper, thus, is to propose a new model for the grid impedance of a planar array of circular disks used to evaluate the frequency behavior of an HIS. Starting from a detailed study of the near-field distribution of the electric field around the circular patches, we modify the analytical formulas already developed for the grid impedance of a squared-patch-based HIS [24, 25] in order to accurately describe the behavior of a circular-patch-based one. The new proposed model is validated considering its ability to reproduce the full-wave numerical results obtained through the commercial electromagnetic simulator CST Studio Suite [26]. As further comparison, we report the results of the frequency response estimated by the other models [21, 23].

The structure of the paper is as follows. In Section 2, we briefly review the model of an HIS and discuss the grid impedance of a circular-patch-based HIS, presenting the related analytical formulas. In Section 3, we show the comparison between the resonant frequencies estimated using the proposed analytical model, the full-wave numerical simulator [26], the sub-wavelength-FSS-based model and the polarizability-based model.

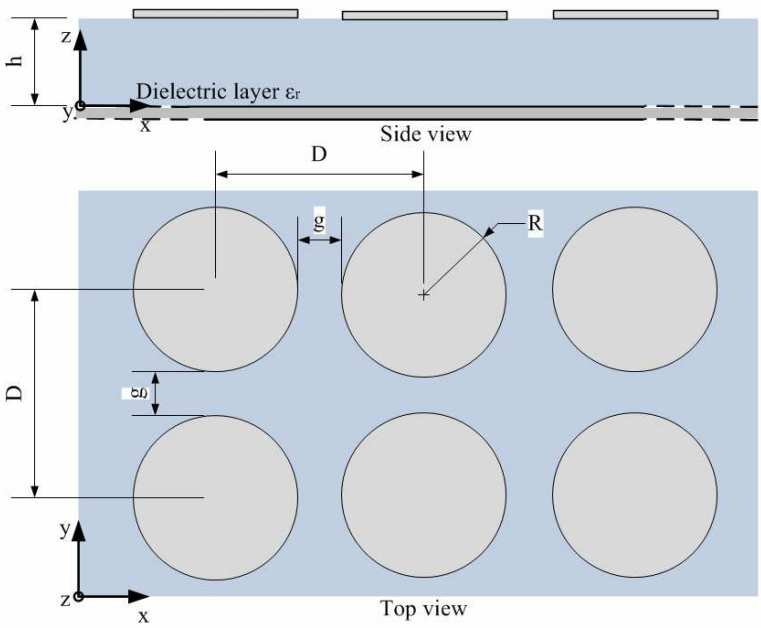


**Figure 1.** Side and top views of an HIS made by a regular array of circular patches.

## 2. ANALYTICAL MODEL

An HIS consisting of a regular array of circular patches is shown in Figure 1. The surface is infinite in the $xy$ plane and the dielectric material considered is non-magnetic, i.e., its permeability is taken to be the free-space permeability $\mu_0$. The thickness and the relative electric permittivity of the dielectric slab are $h$ and $\varepsilon_r$, respectively. The period of the array is $D$ in both directions. The metallic components are assumed to have a negligible thickness. The radius of the patches is $R$, and $g$ is the gap between two adjacent patches.

As well known, the frequency behavior of an HIS can be easily studied using the transmission line model shown in Figure 2.

The metal-backed dielectric slab is equivalent to a transmission line of length $h$ and characteristic impedance $Z_d = Z_0/\sqrt{\varepsilon_r}$, where $Z_0 = 377\,\Omega$ is the free-space wave impedance, terminated in a vanishing impedance $Z_L$ modeling the metallic ground plane. The shunt impedance $Z_g$ represents the averaged impedance of the grid [22], which is a meaningful parameter when the periodicity $D$ is smaller than the operating wavelength. The total surface impedance of the HIS is given by the input impedance $Z_s$ resulting from the parallel connection between the grid impedance $Z_g$ and the line impedance $Z_\ell$:

$$Z_s = \left( \frac{1}{Z_g} + \frac{1}{Z_\ell} \right)^{-1} \tag{1}$$

where the input impedance $Z_s$ exhibits an anti-resonant behavior and the structure shows high values of the surface impedance at and around the resonant frequency.

In order to evaluate the grid impedance $Z_g$, we investigate on the distribution of the electric charges on the array plane when it is illuminated by a plane wave in long-wavelength regime. As shown in Figure 3, the electric charges are distributed along the curved edges

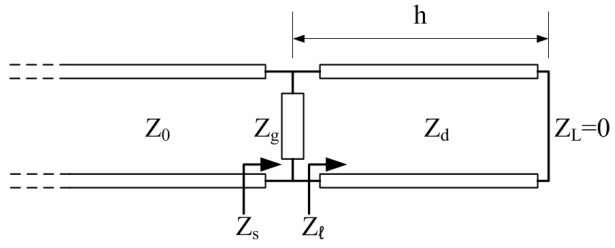


**Figure 2.** Transmission line model of the structure reported in Figure 1.

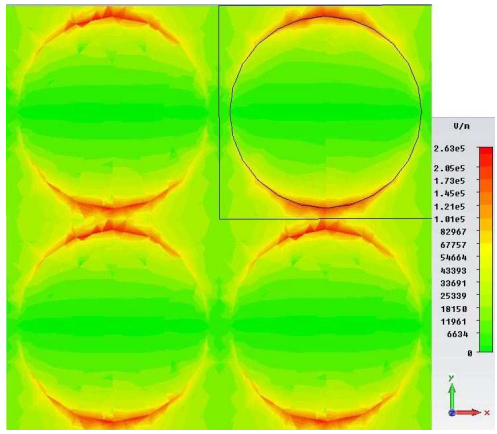


**Figure 3.** Map of the electric field amplitude on the plane of an array of circular patches. The exciting electric field is polarized along the $y$-direction.

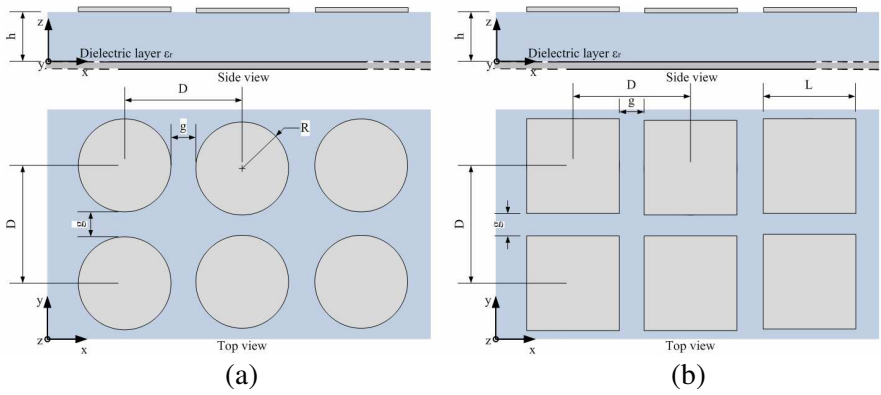


**Figure 4.** Side and top views of an HIS made by a regular array of (a) circular and (b) squared patches.

of the metallic circular elements. In the region of minimum distance between the edges of two adjacent vertical patches the electric field amplitude is maximum.

The distribution of the electric field along the edge is more similar to the one of a squared patch that, under the same condition of excitation, is quite constant along the whole length. In the following we show that, by using a proper modification, the formulas, used for the squared patch case proposed in [24], can be effectively used also for the circular case.

In Figure 4 we show the squared- and the circular-patch-based structures with the respective geometrical parameters. They have the same periodicity $D$ and the same gap $g$. The thickness and the electric permittivity of the dielectric slab are also the same. The diameter $2R$ of the circular patches is equal to the length $L$ of the edge of the squared patches.

When an uniform plane-wave impinges normally on the surface from the above, the grid impedance $Z_g$ of the structure in Figure 4(b) is given by [22, 24, 25]:

$$Z_g = -j\frac{Z_{eff}}{2\alpha} \tag{2}$$

where $\alpha$ is the grid parameter defined as:

$$\alpha = \frac{k_{eff}\,D}{\pi}\ln\left[\frac{1}{\sin\left(\frac{\pi g}{2D}\right)}\right] \tag{3}$$

where $Z_{eff} = Z_0/\sqrt{\varepsilon_{eff}}$ and $k_{eff} = k_0\sqrt{\varepsilon_{eff}}$ are the wave impedance and the wave number in the effective medium, respectively, and $\varepsilon_{eff}$ is the effective permittivity of the space surrounding the array grid. In fact, according to [27, 28], it is possible to analyze the electromagnetic behavior of a structure at the interface between two dielectrics, one of which is the air, using an effective permittivity $\varepsilon_{eff} = (\varepsilon_r+1)/2$ as if the array elements were embedded in an equivalent effective medium. The formula is accurate for periodic structures whose periodicity is smaller than the operating wavelength and presents a slight dependence on the thickness of the substrate since the electric field lines are confined

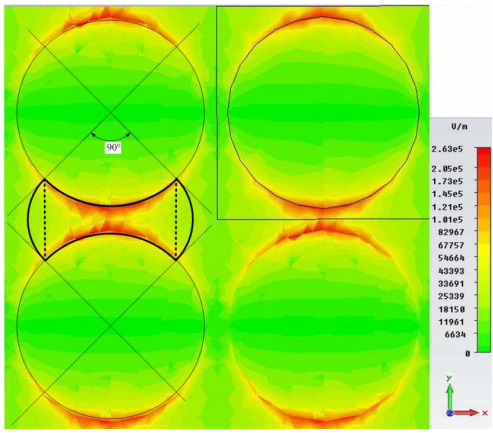


**Figure 5.** Full (solid line) and rectangular (dotted line) integrating regions.

essentially at the air-dielectric interface due to the proximity of the metallic edges (i.e., the metallic ground plane slightly contribute to the definition of the grid impedance of the array).

In order to modify such formulas for the circular patch case, as reported in Figure 5, we observe that it is possible to identify a finite region between two adjacent patches where the electric field amplitude is maximum. By applying the integral mean value theorem over this region, an averaged value of the gap $g$ can be evaluated and used in Equations (2)–(3), rectifying, *de facto*, the circular patch in an equivalent squared one with the same periodicity, but with a different value of the gap $g$. The integration area is shown in Figure 5. The upper and lower integration limits are given by the edges of the

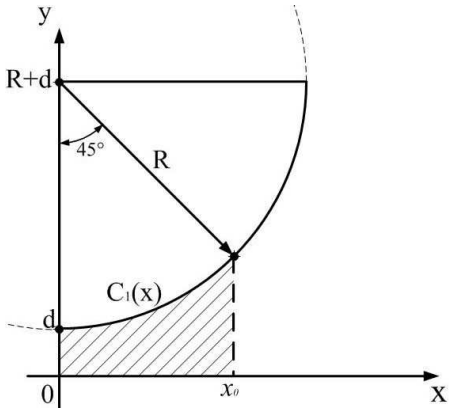


**Figure 6.** Rectangular area of integration.

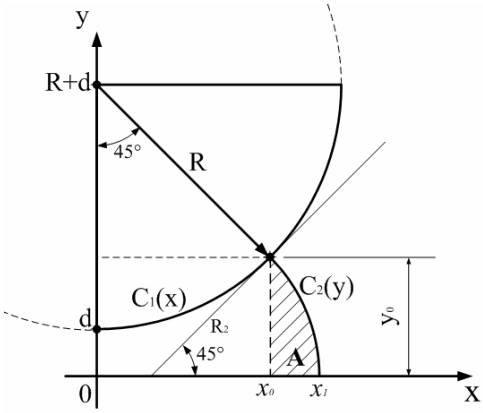


**Figure 7.** Full area of integration.

circular patches, while the right and left boundaries can be defined in two alternative ways, considering either the solid or the dotted lines. Solid lines limit the full region following the curvature of ideal electric field lines intersecting orthogonally the metallic edges. Dotted lines, instead, do not consider this curvature, defining a smaller, and less accurate, rectangular region. In the following, we will consider these two cases separately.

### 2.1. Rectangular Region

In order to determine the area of the rectangular region, we consider only one quarter of the structure, as shown in Figure 6. The origin of the rectangular coordinate system is translated between two adjacent patches. The area is defined using $x$ and $y$ variables as:

$$\begin{cases} 0 \leq x \leq x_0 \\ 0 \leq y \leq C_1(x) \end{cases} \tag{4}$$

where $x_0$ is the maximum value of $x$ in the region of interest and $C_1(x)$ is the function of the arc that identifies the upper limit of the region. The expression of $C_1(x)$ can be found starting from the equation of a circle centered in $\{\bar{x}, \bar{y}\} = \{0, R+d\}$ as:

$$C_1(x) = d + R - \sqrt{R^2 - x^2} \tag{5}$$

The dashed area in Figure 6 is given by:

$$\int_0^{x_0} C_1(x)dx = (d+R)x_0 - \frac{1}{2}\left[R^2 \tan^{-1}\frac{x_0}{\sqrt{R^2 - x_0^2}} + x_0\sqrt{R^2 - x_0^2}\right] \tag{6}$$

Since $x_0 = R/\sqrt{2}$, expression (6) can be simplified as follows:

$$\int_0^{x_0} C_1(x)dx = \frac{1}{8}R\left[4\sqrt{2}d + \left(4\sqrt{2} - 2 - \pi\right)R\right] \tag{7}$$

Now it is possible to evaluate the new averaged value of $d$ between two adjacent patches:

$$\bar{d}_{rect} = \frac{1}{x_0}\int_0^{x_0} C_1(x)dx \tag{8}$$

One can express $x_0$ and $R$ in terms of the periodicity $D$ and of the gap $g$ as:

$$\begin{cases} x_0 = \frac{R}{\sqrt{2}} \\ R = \frac{1}{2}(D - g) \\ g = 2d \end{cases} \tag{9}$$

Using Equation (9) in Equations (7)–(8), we obtain:

$$\bar{g}_{rect} = \frac{\left(4\sqrt{2} - 2 - \pi\right) D + (2 + \pi)g}{4\sqrt{2}} \tag{10}$$

or, evaluating the numerical coefficients:

$$\bar{g}_{rect} \cong 0.91g + 0.09D \tag{11}$$

Such an expression can be straightforwardly employed in formulas (2)–(3) to estimate the behavior of the circular-patch-based HIS.

## 2.2. Full Region

In the case of the full region (Figure 7), the integration area is larger because we consider the area A under the arc of the curve $C_2(y)$, which approximates the electric field lines between two adjacent patches. Being the electric field always orthogonal to metallic surfaces, the arc intersects normally the circumference of the patch. The expression of the curve $C_2(y)$ has been found in the same way as for curve $C_1(x)$ as:

$$C_2(y) = (x_0 - y_0) + \sqrt{R_2^2 - y^2} \tag{12}$$

Only the area A between $C_2(y)$ and $x_0$ is of interest: the integral of the function $C_2'(y)$ (i.e., function $C_2(y)$ shifted by an amount $x_0$) is evaluated as:

$$A = \int_0^{y_0} C_2'(y)dy = \int_0^{y_0} \left(\sqrt{R_2^2 - y^2} - y_0\right) dy \tag{13}$$

which returns:

$$\begin{aligned} A \;=\; & \int_0^{y_0} C_2'(y)dy = -y_0^2 \\ & + \frac{1}{2}\left[y_0\sqrt{R_2^2 - y_0^2} + R_2^2 \tan^{-1}\left(\frac{y_0}{\sqrt{R_2^2 - y_0^2}}\right)\right] \end{aligned} \tag{14}$$

Being $y_0 = R_2/\sqrt{2}$, Equation (14) can be simplified as:

$$A = \int_0^{y_0} C_2'(y)dy = \frac{1}{8}(\pi - 2)R_2^2 \tag{15}$$

The new averaged value of $d$ between two adjacent patches is:

$$\bar{d}_{full} = \frac{1}{x_1}\left[\int_0^{x_0} C_1(x)dx + \int_0^{y_0} C_2'(y)dy\right] \tag{16}$$

where $x_1 = x_0+(\sqrt{2}-1)y_0$. The two integrals in (16) have been already evaluated in Equations (7) and (15). Consequently, one obtains the expression:

$$\bar{d}_{full} = \frac{1}{2x_1}\left[R\left[4\sqrt{2}d + \left(4\sqrt{2}-2-\pi\right)R\right] + (\pi-2)R_2^2\right] \tag{17}$$

Finally, expressing all the factors in terms of the periodicity $D$ and the gap $g$, we obtain:

$$\begin{cases} R_2 = \sqrt{2}(R+d) - R \\ x_1 = (\sqrt{2}-1)(2R+d) \\ R = (D-g)/2 \\ g = 2d \end{cases} \tag{18}$$

and, thus:

$$\bar{g}_{full} = \frac{1}{8(d-D)}\left[2(1+\sqrt{2})g^2 + (\pi-4)D^2 - ((2+\sqrt{2})\pi-4)gD\right] \tag{19}$$

Again, such an expression can be straightforwardly employed in formulas (2)–(3) to estimate the behavior of the circular-patch-based HIS.

## 3. NUMERICAL VALIDATION

In this Section, we compare the analytical results obtained applying the new proposed models to the ones obtained using the numerical results obtained through CST Microwave Studio. As further comparison we show the results obtained using the sub-wavelength-FSS-based model and the polarizability-based model.

The aim is to show that the first expression of the gap, $\bar{g}_{rect}$, though simple, returns good results, but, generally, the second expression of the gap, $\bar{g}_{full}$, allows obtaining more accurate results.

In order to assess the effectiveness of the proposed model, we first consider its ability to predict the resonance frequency of the HIS. To do that, we define the percentage error on the resonance frequency of the HIS as:

$$err\% = \frac{f_r^{mod} - f_r^{sim}}{f_r^{sim}} 100 \tag{20}$$

where $f_r^{sim}$ is the resonance frequency of the structure given by the numerical simulator and $f_r^{mod}$ is the one estimated by the model.

The couples ($D$, $g$), chosen to test the proposed models, have been collected in cases as shown in Table 1.

**Table 1.** Couples of values of periodicity $D$ and gap $g$ of the analyzed structures.

| CASE | $D$ [mm] | $g$ [mm] |
|---|---|---|
| A | 3.0 | 0.30 |
| B | 1.0 | 0.20 |
| C | 4.0 | 0.20 |
| D | 1.5 | 0.05 |
| E | 4.0 | 0.05 |

**Table 2.** Comparison between the resonant frequencies in GHz of 15 different configurations of HISs: $f_r^{sim}$ exact resonant frequency using full-wave simulator; $f_r^{mod}$ using the analytical models.

| Substrate Parameters: $\varepsilon_r$ = 10.2, $h$ = 1.0 mm | | | | | | | | | |
|---|---|---|---|---|---|---|---|---|---|
| Case | $f_r^{sim}$ | Rect-region based | | Full-region based | | FSS-based [21] | | Polarizability-based [23] | |
| | | $f_r^{mod}$ | **err%** | $f_r^{mod}$ | **err%** | $f_r^{mod}$ | **err%** | $f_r^{mod}$ | **err%** |
| A | 11.99 | 11.51 | **-4.0** | 11.87 | **-0.1** | 13.5 | **+12.6** | 15.02 | **+25.3** |
| B | 19.00 | 18.11 | **-4.7** | 18.33 | **-3.5** | 19.2 | **+1.1** | 19.70 | **+3.7** |
| C | 9.44 | 9.38 | **-0.6** | 9.79 | **+3.7** | 10.91 | **+15.6** | 13.45 | **+42.5** |
| D | 13.65 | 13.46 | **-1.4** | 13.9 | **+1.8** | 15.5 | **+13.6** | 16.07 | **+17.7** |
| E | 8.51 | 8.72 | **+2.5** | 9.16 | **+7.6** | 10.4 | **+22.2** | 13.01 | **+52.9** |
| Substrate Parameters: $\varepsilon_r$ = 10.2, $h$ = 2.0 mm | | | | | | | | | |
| Case | $f_r^{sim}$ | Rect-region based | | Full-region based | | FSS-based [21] | | Polarizability-based [23] | |
| | | $f_r^{mod}$ | **err%** | $f_r^{mod}$ | **err%** | $f_r^{mod}$ | **err%** | $f_r^{mod}$ | **err%** |
| A | 7.79 | 7.37 | **-5.4** | 7.53 | **-3.3** | 8.25 | **+5.9** | 8.56 | **+9.9** |
| B | 10.53 | 10.16 | **-3.5** | 10.27 | **-2.5** | 10.54 | **+0.1** | 10.64 | **+1.0** |
| C | 6.46 | 6.22 | **-3.7** | 6.44 | **-0.3** | 7.2 | **+11.5** | 7.73 | **+19.7** |
| D | 8.59 | 8.30 | **-3.4** | 8.52 | **-0.8** | 9.24 | **+7.6** | 9.18 | **+6.9** |
| E | 5.90 | 5.83 | **-1.2** | 6.05 | **+2.5** | 6.87 | **+16.4** | 7.45 | **+26.3** |
| Substrate Parameters: $\varepsilon_r$ = 2.5, $h$ = 2.0 mm | | | | | | | | | |
| Case | $f_r^{sim}$ | Rect-region based | | Full-region based | | FSS-based [21] | | Polarizability-based [23] | |
| | | $f_r^{mod}$ | **err%** | $f_r^{mod}$ | **err%** | $f_r^{mod}$ | **err%** | $f_r^{mod}$ | **err%** |
| A | 14.55 | 13.75 | **-5.5** | 14.1 | **-3.1** | 15.51 | **+6.6** | 16.29 | **+11.9** |
| B | 20.50 | 19.91 | **-2.9** | 20.03 | **-2.3** | 20.74 | **+1.2** | 20.98 | **+2.3** |
| C | 11.97 | 11.45 | **-4.3** | 11.87 | **-0.8** | 13.36 | **+11.6** | 14.58 | **+21.8** |
| D | 16.06 | 15.75 | **-1.9** | 16.16 | **-0.6** | 17.7 | **+10.2** | 17.62 | **+9.7** |
| E | 10.90 | 10.71 | **-1.7** | 11.15 | **+2.3** | 12.72 | **+16.7** | 13.99 | **+28.3** |

Several different structures with different geometrical dimensions and permittivity values have been simulated. The numerical results are compared to the proposed analytical ones, as shown in Table 2 with the header Rect-region based and Full-region based, respectively. In the cases A, B, C, and D the resonance frequency is better predicted by the model that uses the expression $\bar{g}_{full}$ for all the three combinations of permittivity and thickness of the substrate. On the contrary, when the periodicity $D$ of the array is much larger than the separation $g$ (case E), the use of $\bar{g}_{full}$ is not recommended any more. In fact, as shown in Figure 5, the proposed model has been developed considering the region between two adjacent patches under a fixed angle of 90°. On the contrary, in case E, the electric field is strongly confined in the region of minimum distance between two adjacent patches and, when $\bar{g}_{full}$ is evaluated, we overestimate the area in which the electromagnetic energy should be confined. For this reason, $\bar{g}_{rect}$ better predicts the frequency response of the array. However the percentage error is very low for all fifteen configurations, showing the good agreement with the exact full-wave numerical results.

The results of the other analytical models (presented in [21] and [23]) are also shown in Table 2. They both overestimate the resonant frequency of the HIS and return an absolute percentage error

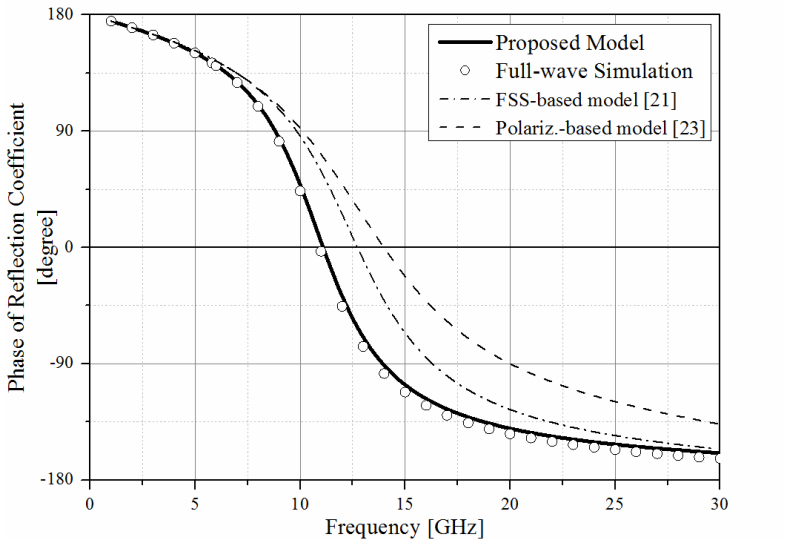


**Figure 8.** Phase of the reflection coefficient of an HIS with circular patches ($D = 4\,\text{mm}$, $g = 0.05\,\text{mm}$, $h = 2\,\text{mm}$ and $\varepsilon_r = 2.5$).

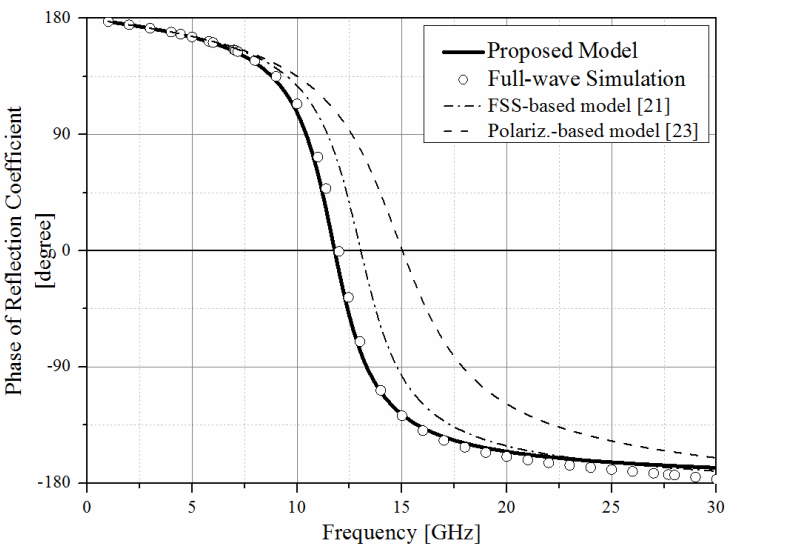


**Figure 9.** Phase of the reflection coefficient of an HIS with circular patches ($D = 3\,\text{mm}$, $g = 0.3\,\text{mm}$, $h = 1\,\text{mm}$ and $\varepsilon_r = 10.2$).

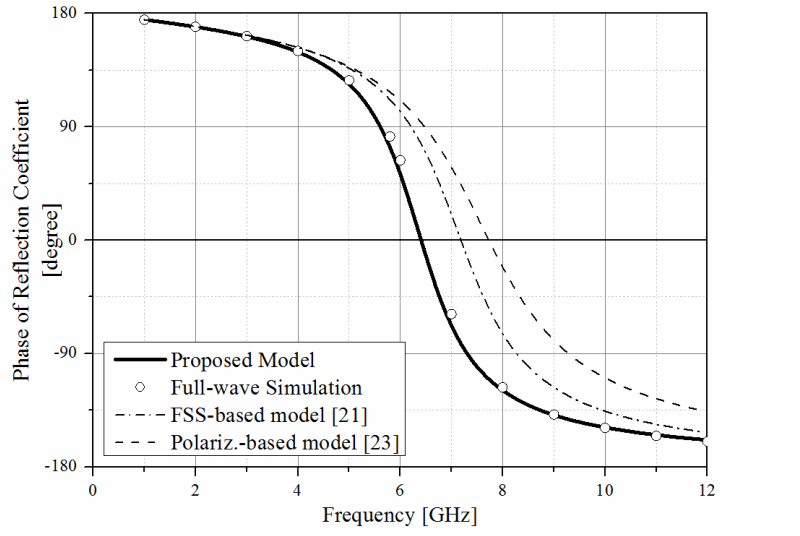


**Figure 10.** Phase of the reflection coefficient of an HIS with circular patches ($D = 4\,\text{mm}$, $g = 0.2\,\text{mm}$, $h = 2\,\text{mm}$ and $\varepsilon_r = 10.2$).

which is generally higher than the one of the proposed method. It is worth noticing that only in the case B the other two analytical models are fairly accurate. In this case, in fact, the ratio $g/D$ is smaller compared to the other cases and, thus, the metallic inclusions are more diluted, as required by the models based on the FSS theory [21] and on the polarizability [23].

Three particular configurations have been chosen among the 15 ones reported in Table 2. For all of them the phase of the reflection coefficient has been evaluated as a function of the frequency and compared to the one obtained through the full-wave code (see Figure 8, 9, 10). The agreement between the proposed model based on the full integrating region and the numerical simulations is rather good in a broad frequency range.

## 4. CONCLUSIONS

In this work, we have presented new accurate analytical formulas for the design of HISs consisting of circular metallic patches excited by a normally impinging plane-wave. The structure can be described using the transmission line theory where a shunt capacitive impedance represents the dense array of circular metallic patches. We have shown that, by inspecting the near-zone electric field distribution around the patches, two sets of new analytical formulas can be derived properly modifying the expression of the grid impedance of a squared-patch-based HIS. They show different degrees of accuracy: the full-region model, which takes into account the curvature of the electric field lines, is generally better, but it gives less accurate results with respect to the rectangular one when the diameter of the patch is much larger than the gap $g$. However, for several different configurations of HIS, it predicts the frequency behavior of the structure with a low percentage error and a rather good agreement with the full-wave simulation in a broad frequency range, confirming its aspect of general purpose.

The analytical results are compared also with two other models, available in the open technical literature: the sub-wavelength-FSS-based model [21], that has been derived approximating the Floquet theory under the assumption that the periodicity is few tenths of the operating wavelength, and the polarizability-based model [23], that assumes the inclusions so electrically small that they can be described in terms of an electric dipoles, losing the information about the geometry of the inclusion itself. Except for one case, the models are not able to describe correctly the frequency behavior of the different HISs.

An improvement of the proposed model can be obtained considering a variable integration angle $\theta$ as a function of the physical dimension of the array inclusions, rather than a fixed angle of 90°. Future works will be focused on this intriguing aspect, providing eventually a more complete formulation involving also the polarization and the angles of incidence of the impinging plane-wave.

## REFERENCES

1. Bilotti, F., A. Toscano, and L. Vegni, "FEM-BEM formulation for the analysis of cavity backed patch antennas on chiral substrates," *IEEE Trans. Antennas Propagat.*, Vol. 51, 306–311, 2003.
2. Bilotti, F., A. Toscano, and L. Vegni, "Radiation and scattering features of patch antennas with bianisotropic substrates," *IEEE Trans. Antennas Propagat.*, Vol. 51, 449–456, 2003.
3. Scamarcio, G., F. Bilotti, A. Toscano, and L. Vegni, "Broad band U-slot patch antenna loaded by chiral material," *Journal of Electromagnetic Waves and Applications*, Vol. 15, No. 10, 1303–1317, 2001.
4. Bilotti, F. and L. Vegni, "Chiral cover effects on microstrip antennas," *IEEE Trans. Antennas Propagat.*, Vol. 51, 2891–2898, 2003.
5. Vegni, L., A. Toscano, and F. Bilotti, "Shielding and radiation characteristics of planar layered inhomogeneous composites," *IEEE Trans. Antennas Propagat.*, Vol. 51, 2869–2877, 2003.
6. Ziolkowski, R. W. and N. Engheta, "Metamaterial special issue introduction," *IEEE Trans. Antennas Propagat.*, Vol. 51, No. 10, 2546–2549, 2003.
7. Vardaxoglou, J. C., *Frequency Selective Surfaces: Analysis and Design*, Research Studies Press, Taunton, England, 1997.
8. Bilotti, F., A. Alù, N. Engheta, and L. Vegni, "Anomalous properties of scattering from cavities partially loaded with double-negative or single-negative metamaterials," *Progress In Electromagnetics Research*, Vol. 51, 49–63, 2005.
9. Bilotti, F., L. Nucci, and L. Vegni, "An SRR based microwave absorber," *Microw. Opt. Technol. Lett.*, Vol. 48, 2171–2175, 2006.
10. Bilotti, L., A. Toscano, L. Vegni, K. B. Alici, K. Aydin, and E. Ozbay, "Equivalent circuit models for the design of metamaterials based on artificial magnetic inclusions," *IEEE Trans. Microw. Theory Tech.*, Vol. 55, 2865–2873, 2007.

11. Alù, A., F. Bilotti, N. Engheta, and L. Vegni, "Sub-Wavelength planar leaky-wave components with metamaterial bilayers," *IEEE Trans. Antennas Propagat.*, Vol. 55, 882–891, 2007.
12. Bilotti, F., S. Tricarico, and L. Vegni, "Electromagnetic cloaking devices for TE and TM polarizations," *New J. Phys.*, Vol. 10, 115035, 2008.
13. Bilotti, F., A. Toscano, K. B. Alici, E. Ozbay, and L. Vegni, "Design of miniaturized narrowband absorbers based on resonant magnetic inclusions," *IEEE Trans. Electromag. Comp.*, Vol. 53, 63–72, Feb. 2011.
14. Ramaccia, D., F. Bilotti, and A. Toscano, "Analytical model of a metasurface consisting of a regular array of subwavelenght circular holes in a metal sheet," *Progress In Electromagnetics Research M*, Vol. 18, 209–219, 2011.
15. Sievenpiper, D., L. Zhang, R. F. J. Broas, N. Alexopolous, and E. Yablonovitch, "High-impedance electromagnetic surfaces with a forbidden frequency band," *IEEE Trans. Microw. Theory Tech.*, Vol. 47, 2059–2074, 1999.
16. Sievenpiper, D., "High-impedance electromagnetic surfaces," Ph.D. Dissertation, UCLA, 1999. Available at www.ee.ucla.edu/labs/photon/thesis/ThesisDan.pdf.
17. De Cos, M. E., Y. Alvarez Lopez, and F. Las-Heras Andrés, "A novel approach for RCS reduction using a combination of artificial magnetic conductors," *Progress In Electromagnetics Research*, Vol. 107, 147–159, 2010.
18. Chang, C.-S., J.-Y. Li, W.-J. Lin, M.-P. Houng, L.-S. Chen, and D.-B. Lin, "Controlling the frequency of simultaneous switching noise suppression by using embedded dielectric resonators in high-impedance surface structure," *Progress In Electromagnetics Research Letters*, Vol. 11, 149–158, 2009.
19. De Cos, M. E., Y. Alvarez Lopez, R. C. Hadarig, and F. Las-Heras Andrés, "Flexible uniplanar artificial magnetic conductor," *Progress In Electromagnetics Research*, Vol. 106, 349–362, 2010.
20. Sievenpiper, D., E. Yablonovitch, J. N. Winn, S. Fan, P. R. Villeneuve, and J. D. Joannopoulos, "3D metallo-dielectric photonic crystals with strong capacitive coupling between metallic islands," *Phys. Rev. Lett.*, Vol. 80, 2829–2832, 1998.
21. Zarrillo, G. and K. Aguiar, "Closed-form low frequency solutions for electromagnetic waves through a frequency selective surface," *IEEE Trans. Antennas Propagat.*, Vol. 35, No. 12, 1987.

22. Tretyakov, S. A., *Analytical Modeling in Applied Electromagnetics*, Artech House, Norwood, MA, 2003.
23. Viitanen, A. J., I. Hanninen, and S. A. Tretyakov, "Analytical model for regular dense arrays of planar dipole scatterers," *Progress In Electromagnetics Research*, Vol. 38, 97–110, 2002.
24. Luukkonen, O., C. R. Simovsky, G. Granet, G. Goussetis, D. Lioubtchenko, A. Raisanen, and S. A. Tretyakov, "Simple and accurate analytical model of planar grids and high-impedance surfaces comprising metal strips," *IEEE Trans. Antennas Propagat.*, Vol. 56, 1624–1632, 2008.
25. Lee, S., G. Zarrillo, and C. L. Law, "Simple formulas for transmission trough periodic metal grids or plattes," *IEEE Trans. Antennas Propagat.*, Vol. 30, No. 5, 1982.
26. CST Studio Suite 2010, Computer Simulation Technology, http://www.cst.com.
27. Compton, R. C., L. B. Whitbourn, and R. C. McPhedran, "Strip gratings at a dielectric interface and applications of Babinet's principle," *Appl. Opt.*, Vol. 23, 3236–3242, 1984.
28. Timusk, T. and P. L. Richards, "Near millimeter wave bandpass filters," *Appl. Opt.*, Vol. 20, 1355–1360, 1981.